

Insights into Formate Oxidation by a Series of Cobalt Piano-Stool Complexes Supported by Bis(phosphino)amine Ligands

Andrew W. Cook, Thomas J. Emge, and Kate M. Waldie*

Cite This: <https://doi.org/10.1021/acs.inorgchem.1c00563>

Read Online

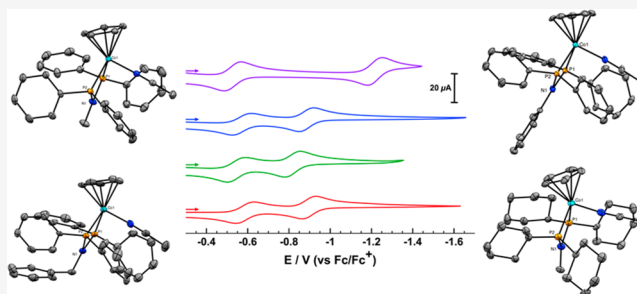
ACCESS |

Metrics & More

Article Recommendations

Supporting Information

ABSTRACT: A series of (cyclopentadienyl)cobalt(III) half-sandwich complexes (1–4) supported by bidentate bis(phosphino)amine ligands was synthesized and characterized by NMR spectroscopy, X-ray crystallography, and cyclic voltammetry. The Co^{III}-hydride complex 4-H bearing the bis(cyclohexylphosphine) ligand derivative was successfully isolated via protonation of the neutral reduced Co^I complex 5 with a weak acid. Experimental and computational methods were used to determine the thermodynamic hydride accepting ability of these Co^{III} centers and to evaluate their reactivity toward the oxidation of formate. We find that the hydride accepting ability of 1–4 ranges from 71 to 74 kcal/mol in acetonitrile, which should favor a highly exergonic reaction with formate through direct hydride transfer. Formate oxidation was demonstrated at elevated temperatures in the presence of stoichiometric quantities of 4, generating carbon dioxide and the Co^{III}-hydride complex 4-H in 72% yield.



Formate oxidation was demonstrated at elevated temperatures in the presence of stoichiometric quantities of 4, generating carbon dioxide and the Co^{III}-hydride complex 4-H in 72% yield.

INTRODUCTION

The storage of renewable energy, such as solar and wind, in chemical bonds offers a promising means of addressing the intermittency of these power sources. Hydrogen has been the subject of intense investigation in this regard given its carbon-free nature and unsurpassed gravimetric energy density (Figure 1).¹ However, the low volumetric energy density of gaseous hydrogen necessitates its pressurization or liquification, which will require significant infrastructure development for its safe transport and on-board storage.² As such, liquid fuels that can be reversibly (de)hydrogenated to serve as H₂ storage carriers or used directly in non-H₂ fuel cells are especially appealing.^{3,4}

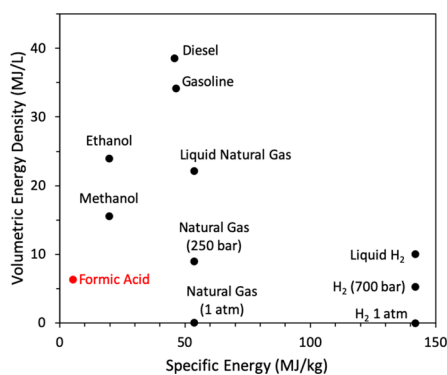


Figure 1. Volumetric energy density versus specific energy of select chemical fuels. Modified from refs 3 and 4.

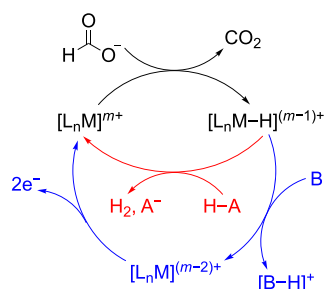
Formic acid is a particularly attractive candidate for this purpose, and there have been significant advances in both the catalytic dehydrogenation of formic acid and the electrocatalytic oxidation of formate.^{1,5–8} However, current heterogeneous systems that exhibit the best performance are generally based on precious metals, such as Ir, Ru, Pt, and Pd, which is cost prohibitive for large scale implementation.^{1,5–8} Additionally, catalyst poisoning by carbon monoxide, the product of formic acid dehydration, is problematic due to the poor selectivity of heterogeneous systems. Homogeneous catalysts based on first-row transition metals may ameliorate these issues by enhancing selectivity while using lower-cost metals and maintaining high efficiency. Indeed, several formic acid oxidation catalysts based on Fe and Mn have been recently reported that utilize tripodal phosphine⁹ or phosphine-based PNP pincer ligands,^{10–13} while the only first-row transition metal catalyst reported for the electrocatalytic oxidation of formate is based on Ni with phosphine ligands containing pendent amine groups.¹⁴

The proposed mechanism for formate oxidation generally involves a metal–hydride complex as a key intermediate, which is generated via hydride transfer from formate to the metal

Received: February 24, 2021

(Scheme 1).^{8,10–24} Subsequent protonation of the metal–hydride intermediate creates a scheme for formic acid

Scheme 1. Proposed Mechanism for the Thermal (Red Path) or Electrochemical (Blue Path) Oxidation of Formate



dehydrogenation, while oxidative deprotonation of the metal–hydride would enable an electrocatalytic cycle (Scheme 1). Notably, a common feature in many of the aforementioned oxidation catalysts is the presence of phosphine ligands that incorporate an amine^{10,13,14} or amide functionality.^{11,12} Mechanistic studies have shown that these pendent proton-active groups play an important role in the intramolecular movement of hydrogen as well as stabilizing key transition states.^{10–14,25,26} Thus far, ligand architectures based on methylene or ethylene connections between the P and N atoms have been explored, while bis(phosphines) bridged solely by an amine group have yet to be investigated. Such bis(phosphino)amine ligands have proven useful in organometallic catalysis with first-row transition metals for cross-coupling and cyclization reactions,^{27–29} hydrogen evolution,^{30–32} and ethylene polymerization.^{33–36}

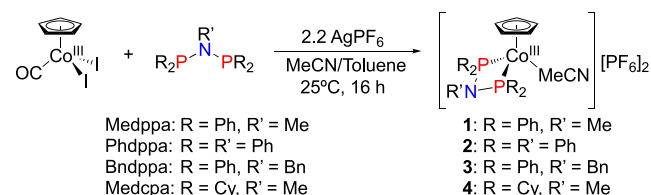
The thermodynamic hydricity (ΔG_{H^-}) of formate in acetonitrile is 44 kcal/mol,^{37–39} and thus a metal complex must have a greater hydride accepting ability in order to favor exergonic formate oxidation. Given the large hydride affinities typically observed for Co^{III}-based hydrogen evolution catalysts,^{39–46} we posited that the Co^{III} center in [(PNP)CpCo(MeCN)]²⁺ “piano-stool” complexes (Cp = cyclopentadienyl, PNP = bis(phosphino)amine) should act as a hydride acceptor and provide a large thermodynamic driving force for the oxidative release of CO₂ from formate. Herein, we report the synthesis and characterization of a series of Co^{III} complexes 1–4 bearing bis(phosphino)amine ligands and assess their efficacy for formate oxidation. The thermodynamic hydricity of the corresponding Co^{III}–hydride complexes is determined using their pK_a values and the reduction potentials of 1–4. We demonstrate that complex 4 with a cyclohexylphosphine-substituted ligand facilitates hydride transfer from formate at elevated temperatures. Additionally, independent preparation of the Co^I (5) and Co^{III}–hydride (4-H) analogs of 4 coupled with theoretical computations provide insights into the equilibria taking place during this reaction.

RESULTS AND DISCUSSION

Synthesis. The bis(phosphino)amine ligands used in this study, bis(diphenylphosphino)methylamine (Medppa), bis(diphenylphosphino)phenylamine (Phdppa), bis(diphenylphosphino)benzylamine (Bndppa), and bis(dicyclohexylphosphino)methylamine (Medcpa), were synthesized according to literature procedures.^{35,36,47,48} The syntheses of the bis(phosphino)amine Co complexes 1–4

were carried out according to the literature procedure for related complexes (Scheme 2).⁴⁹ Briefly, oxidation of [CpCo-

Scheme 2. Synthesis of Bis(phosphino)amine Cobalt Complexes 1–4



(CO)₂] with I₂ in diethyl ether yields the Co^{III} half-sandwich di-iodide complex [CpCo(CO)I₂] as a dark powder. This Co precursor was dissolved in acetonitrile, and the phosphine ligand (PNP, 1 equiv) was added as a solid (PNP = Medppa) or as a toluene solution (PNP = Phdppa, Bndppa, Medcpa) to generate [(PNP)CpCo]I as a dark solution *in situ*. Subsequent halide abstraction with AgPF₆ (2.2 equiv) affords complexes 1–4 as moderately air stable orange powders in decent yields after 16 h. Complexes 1–4 are very soluble in acetonitrile and insoluble in dichloromethane and less polar solvents.

The ¹H NMR spectra of 1–4 in MeCN-*d*₃ (Figures S1, S5, S9, and S13) are diamagnetic, with the chemical shift of the Cp resonance being nearly invariant with respect to the identity of the PNP ligand, ranging between 5.72 and 5.83 ppm. These data are in good agreement with previously reported octahedral, low-spin d⁶ Co^{III} half-sandwich complexes with bidentate nitrogen or phosphine ligands.^{45,49–56} Complexes 1 and 4 both exhibit a triplet resonance at δ 3.02 and 2.09 ppm with ³J_{PH} = 10 and 8 Hz, respectively, which are assigned to the *N*-methyl group on the ligand backbone. A similar triplet signal is observed in the ¹H NMR spectrum of 3 at δ 4.66 ppm with ³J_{PH} = 13 Hz and is assigned to the methylene protons of the *N*-benzyl group. The ³¹P{¹H} NMR spectra (Figures S2, S6, S10, and S14) of 1–4 reveal a downfield singlet at ca. 78 ppm for 1–3 and 94 ppm for 4 from the PNP ligand, as well as a characteristic septet at –144.63 ppm from the [PF₆][–] anion.

We attempted to synthesize the Co^I and Co^{III}–hydride analogs of these complexes following reported procedures;^{44,57,58} however, only [(Medcpa)CpCo] (5) and [(Medcpa)CpCoH][PF₆] (4-H) were isolable. To generate 5, [CpCo(CO)₂] and Medcpa (1 equiv) were dissolved in toluene and refluxed for 4 h to give a brown solution (Scheme 3a). Workup of the reaction mixture gives red crystals of 5 in 63% yield. Protonation of 5 with NH₄PF₆ (1 equiv) in tetrahydrofuran immediately produces a bright yellow solution

Scheme 3. Synthesis of (a) 5 and (b) 4-H

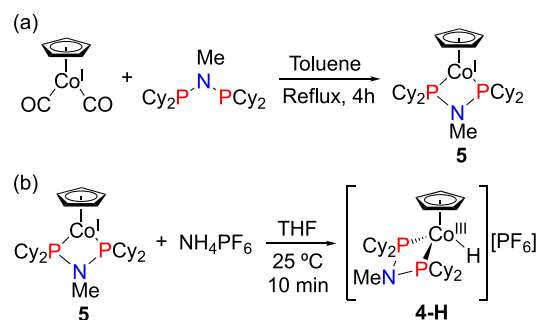


Table 1. Selected Bond Lengths and Angles for 1–5

	1	2	3	4	5
	bond lengths (Å)				
Co1–P (avg.)	2.20	2.21	2.20	2.22	2.11
Co1–N1	2.834(2)	2.866(3)	2.853(2)	2.855(6)	2.825(2)
P1–P2	2.603(1)	2.615(1)	2.578(8)	2.621(2)	2.522(1)
N1–P (avg.)	1.69	1.70	1.67	1.69	1.71
	bond angles (deg)				
P1–Co1–P2	72.4	72.8	71.6	72.3	73.8
ΣN	358.9	359.8	359.7	359.6	360

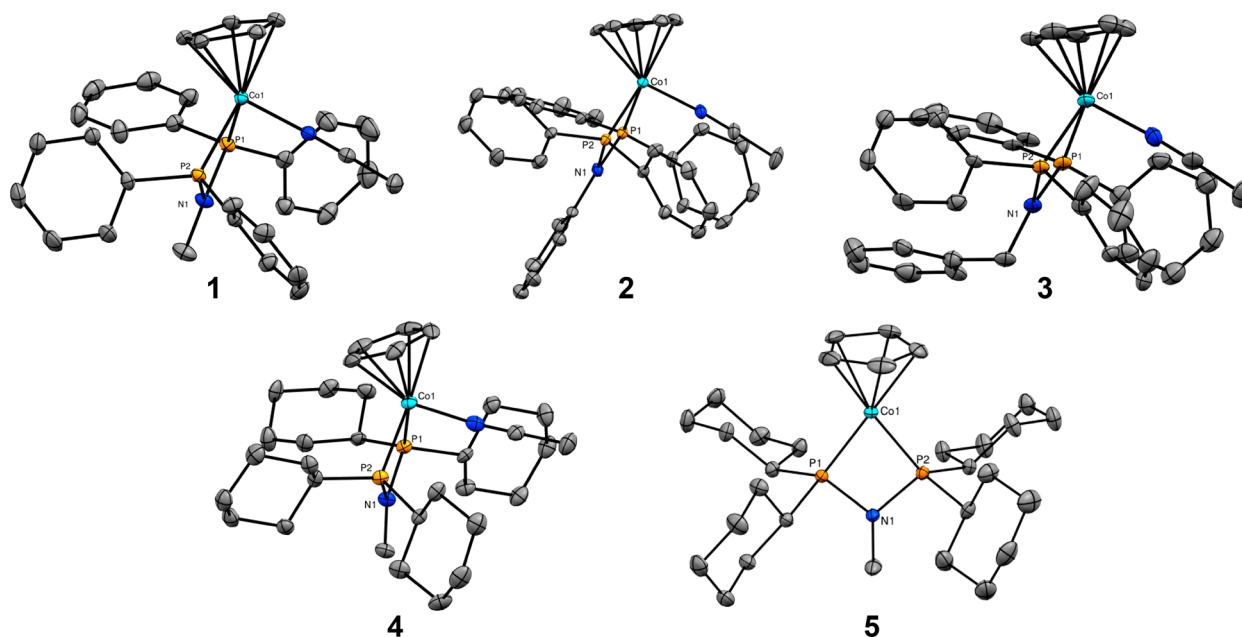


Figure 2. Single crystal X-ray structures of **1**, **2**, **4**, and **5** as well as one independent molecule of **3** shown with 50% probability ellipsoids. Hydrogen atoms, the second molecule of **3**, hexafluorophosphate anions, and cocrystallized solvent molecules are omitted for clarity.

(Scheme 3b), from which **4-H** was obtained as pale-yellow crystals in 81% yield. Complex **5** is soluble in benzene, toluene, tetrahydrofuran, and dichloromethane; very sparingly soluble in diethyl ether and acetonitrile; and insoluble in hexanes. **4-H** is soluble in acetonitrile, partially soluble in tetrahydrofuran, and insoluble in chlorinated and less polar solvents. Attempts to isolate the Co^{I} states of **1–3** in a similar manner led to an intractable mixture of products. The addition of a weak acid, such as NH_4PF_6 , to these mixtures did result in the formation of a small amount of the corresponding Co^{III} –hydride, as observed by ^1H NMR, but these species underwent decomposition in solution to give unidentified products and cyclopentadiene.

The ^1H NMR spectrum of **5** (Figure S17) is diamagnetic, which is consistent with a low-spin Co^{I} formulation. Given the increased electron density and decreased overall charge of the reduced species **5**, the Cp and methyl resonances are significantly shifted upfield compared to **4**, at 4.84 and 2.15 ppm, respectively. This shielding effect upon reduction of the metal center has been previously observed for other half-sandwich metal complexes.^{44,55,57,59} The $^{31}\text{P}\{^1\text{H}\}$ NMR spectrum of **5** (Figure S18) reveals a resonance due to the Medcpa ligand at 104.65 ppm, slightly downfield compared to that of the Co^{III} complex **4**. The ^1H NMR spectrum of **4-H** (Figure S20) shows a downfield shift for both the Cp and methyl resonances to 5.16 and 2.62 ppm, respectively,

consistent with the increased charge of **4-H** versus **5**. Additionally, a new triplet signal appears at -14.02 ppm with $^2J_{\text{PH}} = 68$ Hz, which is diagnostic of the Co^{III} –hydride. The $^{31}\text{P}\{^1\text{H}\}$ NMR spectrum of **4-H** (Figure S21) shows that the Medcpa ligand resonance is shifted further downfield to 118.15 ppm and again shows the characteristic septet at -144.92 ppm from the $[\text{PF}_6]^-$ anion, consistent with the monocationic charge of **4-H**. These chemical shifts are all in good agreement with similar half-sandwich Co^{III} –hydride complexes.^{44,57,58}

Characterization. Solid-State Molecular Structure. Crystals suitable for X-ray crystallographic characterization were obtained through slow diffusion of diethyl ether into a saturated acetonitrile solution at -35 °C. A summary of selected bond lengths and angles is presented in Table 1, and the structures of complexes **1–5** are given in Figure 2. Complexes **1**, **2**, and **4** crystallize as the acetonitrile solvates **1**·MeCN, **2**·MeCN, and **4**·MeCN with one independent molecule in the unit cell, whereas **3** crystallizes as the acetonitrile solvate **3**·0.25MeCN with two independent molecules of **3** in the unit cell. **5** crystallizes without solvation.

Complexes **1–4** are nearly isostructural, with each complex exhibiting a three-legged “piano-stool” geometry around the Co center with a planar η^5 -cyclopentadienyl ligand, bidentate phosphine ligand, and monodentate acetonitrile ligand. To the best of our knowledge, there are only two other structurally

characterized Co^{III} half-sandwich complexes containing a bidentate phosphine ligand with either a methylene or amine bridge: [CpCo(dppm)I]I (dppm = bis(diphenylphosphino)-methane) and [(C₅Me₄H)CoH(Medppa)][PF₆].^{51,58} The Co–P bond distances and P–Co–P bond angles are very similar to these reported structures; however, the P–P distances are intermediate between [CpCo(dppm)I]I (2.690(0) Å) and [(C₅Me₄H)CoH(Medppa)][PF₆] (2.569(2) Å). Additionally, the P–N bond distances are somewhat shorter than what has been observed for the free bis(phosphino)amine ligands and are consistent with [(C₅Me₄H)CoH(Medppa)][PF₆].^{58,60–62} The sum of the angles about the ligand nitrogen center is nearly 360° in 1–4. This nearly trigonal planar geometry at the nitrogen suggests that the amine nucleophilicity is significantly reduced compared to trialkylamines.

Unlike the dicationic Co^{III}–acetonitrile complexes, the neutral Co^I species 5 exhibits a two-legged “piano-stool” geometry about the Co center where the metal is ligated by only the η⁵-cyclopentadienyl and the bidentate phosphine ligands. To the best of our knowledge, this is the first example of a structurally characterized two-legged “piano-stool” Co complex containing a bis(phosphino)amine ligand. The Co–P bond distances are slightly contracted compared to the oxidized complex 4, which is consistent with a greater extent of π-backbonding from the reduced metal center.^{54,63} Similarly, the P–N bonds are slightly elongated, suggesting modest weakening of these bonds. The P–Co–P angle and the sum of the angles about the nitrogen in the ligand backbone do not vary significantly between 4 and 5.

Electrochemistry. Cyclic voltammetry (CV) measurements of complexes 1–4 were collected in acetonitrile using [NBu₄][PF₆] as supporting electrolyte and referenced against the ferrocene/ferrocenium (Fc/Fc⁺) redox couple (Table 2,

Table 2. Cyclic Voltammetry Data for 1–4^a

complex	$E_{1/2}^b$ (V)	ΔE_p^c (mV)	i_a/i_c^d	$E_{1/2}^b$ (V)	ΔE_p^c (mV)	i_a/i_c^d
1	−0.59	90	1.04	−0.90	70	1.04
2	−0.55	90	1.06	−0.82	75	1.01
3	−0.57	90	1.03	−0.89	70	1.01
4	−0.53	80	1.08	−1.22	70	1.12

^aConditions: 1 mM [Co] in 0.1 M [NBu₄][PF₆] in acetonitrile, glassy carbon working electrode, Pt counter electrode, Ag/Ag⁺ reference electrode, 100 mV/s. ^b $E_{1/2} = (E_{pa} + E_{pc})/2$ where E_{pa} and E_{pc} are anodic and cathodic peak potentials, respectively. Potentials versus Fc/Fc⁺. ^c $\Delta E_p = E_{pa} - E_{pc}$. ^d i_a = anodic peak current, i_c = cathodic peak current. Determined from the CV shown in Figure 3.

Figure 3). Each complex displays two, reversible reduction events, E_1 and E_2 , at approximately −0.5 V and −0.8 to −1.2 V vs Fc/Fc⁺, which are assigned to the Co^{III/II} and Co^{II/I} couples based on previously reported Co half-sandwich systems with bidentate phosphine ligands.^{44,45,54,57} The ratio of the anodic to cathodic peak currents is approximately one for both redox couples of 1–4, confirming the reversibility of these electrochemical events. Additionally, the linear dependence of both the anodic and cathodic peak currents on the square root of the scan rate ($\nu^{1/2}$) confirms the freely diffusing nature of these species in solution (Figures S51, S54, S57, and S60).

Neither E_1 nor E_2 varies considerably between 1–3, which suggests that the amine substituent only marginally contributes to the electronic structure of these species. In contrast, there is

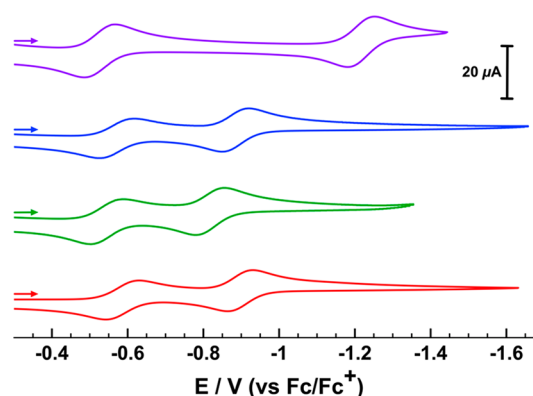
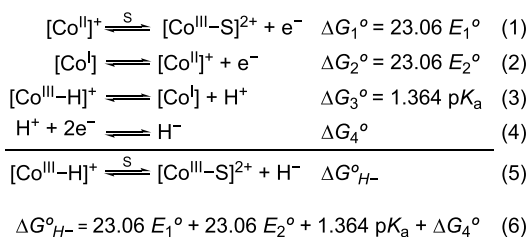


Figure 3. Cyclic voltammograms of 1 (red trace), 2 (green trace), 3 (blue trace), and 4 (purple trace) in acetonitrile (1 mM [Co] and 0.1 M [NBu₄][PF₆]; scan rate = 100 mV/s).

a clear shift in the reduction potentials when the phosphine substituents are changed from phenyl in complex 1 to cyclohexyl in complex 4; thus, the electronic structure is more significantly dictated by the electron donating ability of the phosphine. This effect has been previously found by Artero and co-workers for a series of [CpCo(P₂^RN₂^{R'})I]I complexes (P₂^RN₂^{R'} = 1,5-diaza-3,7-diphosphacyclooctane; R = Cy, Ph; R' = Bn, Ph) complexes.⁴⁵ To our surprise, the first reduction event for 4 occurs at a slightly more positive potential (−0.53 V vs Fc/Fc⁺) than for 1–3, despite the greater electron donating ability of cyclohexylphosphine. However, the second reduction process exhibits the expected significant cathodic shift compared to complexes 1–3.

Thermodynamic Hydricity. On the basis of the H₂ evolution activity of various cobalt catalysts, Co^{III}–hydrides are generally considered to be weakly hydridic, although the hydride donating ability of Co^{III}–hydride complexes has rarely been quantified. One example is the related compound [CpCo(dppe)H][PF₆] with $\Delta G_{H^-} = 71.5$ kcal/mol, which was calculated based on the work of Dempsey and co-workers.^{39,44} To establish the potential utility of 1–4 for formate oxidation via a hydride transfer route, the hydride accepting ability of 1–4 was determined via the potential-pK_a method (Scheme 4).⁶⁴ Note that the hydride accepting ability

Scheme 4. Thermochemical Cycle for the Hydricity of 1-H–4-H

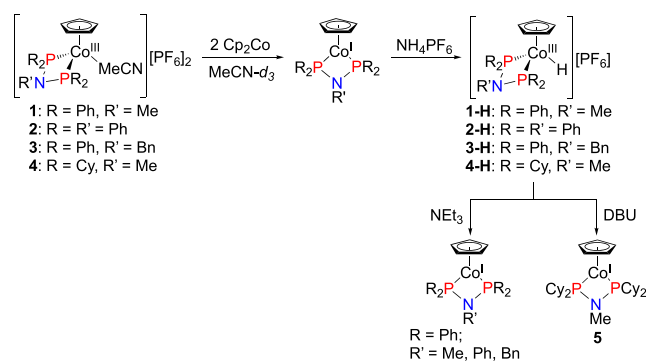


of the Co^{III}–acetonitrile complexes is equal to $-\Delta G_{H^-}$ of the analogous Co^{III}–hydrides. The standard free energies for eqs 1 and 2 are obtained from the E_1 and E_2 reduction potentials of 1–4, measured by CV (Table 2). The standard free energy for the two-electron reduction of H⁺ to H[−] (Scheme 4, eq 4) is 79.6 kcal/mol in acetonitrile.⁶⁴ To complete the thermochemical cycle for hydricity determination, we sought to measure the pK_a of the Co^{III}–hydride complexes (Scheme 4, eq 3).

Spectrophotometric titration of an appropriate base into a solution containing a metal–hydride complex has been used to accurately determine the pK_a of several metal–hydrides.⁴⁴ Here, metered addition of DBU (DBU = 1,8-diazabicyclo[5.4.0]undec-7-ene, $pK_a = 24.31$ in acetonitrile)⁶⁵ to an acetonitrile solution containing 0.9 mM of **4-H** resulted in deprotonation of the hydride complex and the production of its conjugate base **5**, as indicated by an increase in the absorbance at 350 and 461 nm (Figure S48). These data were used to obtain a $pK_a = 23.15$ for **4-H**, and subsequently using eq 6 we obtain $\Delta G_{\text{H}^-} = 71.0$ kcal/mol for **4-H** in acetonitrile.

Unfortunately, the hydride analogs of **1–3** could not be isolated due to instability (*vide supra*); however, an approximate limiting value for their pK_a was estimated by generation of the Co–hydride on an NMR scale followed by rapid deprotonation *in situ* with an appropriate base (Scheme 5, see Supporting Information for Experimental Details). The

Scheme 5. In Situ Generation and Deprotonation of Co^{III}–Hydrides **1-H–4-H**



pK_a of **4-H** was also estimated in this manner to ensure the veracity of these measurements. Briefly, **1–4** were reduced with 2 equiv of cobaltocene in MeCN- d_3 , followed by *in situ* protonation with NH_4PF_6 (1 equiv) to generate the Co^{III}–hydride, which was confirmed by ^1H NMR (Figures S26, S28, S30, and S32). To establish an upper pK_a limit for these complexes, 1 equiv of base with a known pK_a in acetonitrile was quickly added to the sample. Treatment of **1-H**, **2-H**, and **3-H** with triethylamine (1 equiv, $pK_a = 18.83$ in acetonitrile)⁶⁵ led to rapid and quantitative deprotonation of the hydride, giving an upper limit for the hydricity according to eq 6: $\Delta G_{\text{H}^-} = 71.0$, 73.8, and 71.7 kcal/mol for **1-H**, **2-H**, and **3-H**, respectively. Deprotonation of **4-H** was obtained by the addition of 1 equiv of DBU, which gives $\Delta G_{\text{H}^-} = 72.5$ kcal/mol and is in excellent agreement with our spectrophotometrically determined value (*vide supra*). We note that the relatively small variation in these estimated hydricity values is unsurprising given the similarity of the first reduction potentials for **1–4** and the strong correlation between E_1 of the parent metal complex and the thermodynamic hydricity of the corresponding hydride species.³⁹

Reactivity with Formate. The measured hydride accepting ability of **1–4** is sufficiently large to provide considerable thermodynamic driving force for the oxidation of formate and formation of the corresponding Co–hydride. However, the kinetics of hydride transfer to a first-row transition metal can often be sluggish despite favorable reaction energetics. To overcome this kinetic barrier, first-row transition metal catalysts for formic acid dehydrogenation^{8,10–13} or formate

electro-oxidation¹⁴ often utilize an amide or amine functionality to assist in the hydride transfer step. Given this precedent, we probed the stoichiometric reaction of **1–4** with formate.

Treatment of **1–3** with one equivalent of formate (added as the soluble biformate salt, $[\text{NBu}_4][\text{HCO}_2]\cdot\text{HCO}_2\text{H}$) in MeCN- d_3 at 25 °C immediately resulted in a color change from orange to dark brown with concomitant deposition of an intractable dark powder and disappearance of all resonances associated with **1–3** in the ^1H NMR spectra. Additionally, new signals at 6.56, 6.47, and 2.97 ppm appear, consistent with noncoordinated cyclopentadiene. On the other hand, the reaction of **4** with $[\text{NBu}_4][\text{HCO}_2]\cdot\text{HCO}_2\text{H}$ (1.25 equiv) in MeCN- d_3 at 25 °C does not result in the formation of solids and the ^1H NMR immediately reveals new diamagnetic signals (Figures 4, S34, and S35, see Supporting Information for

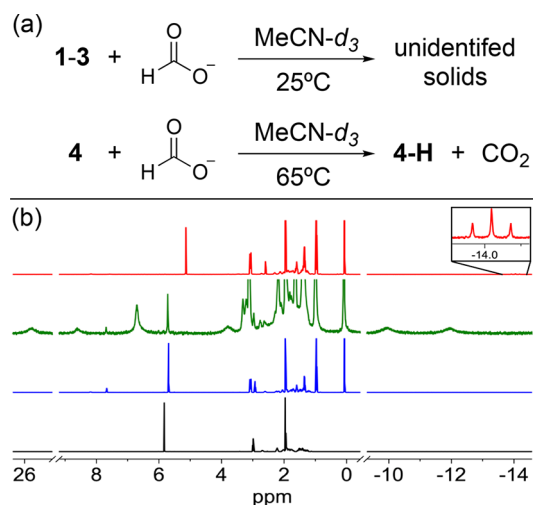


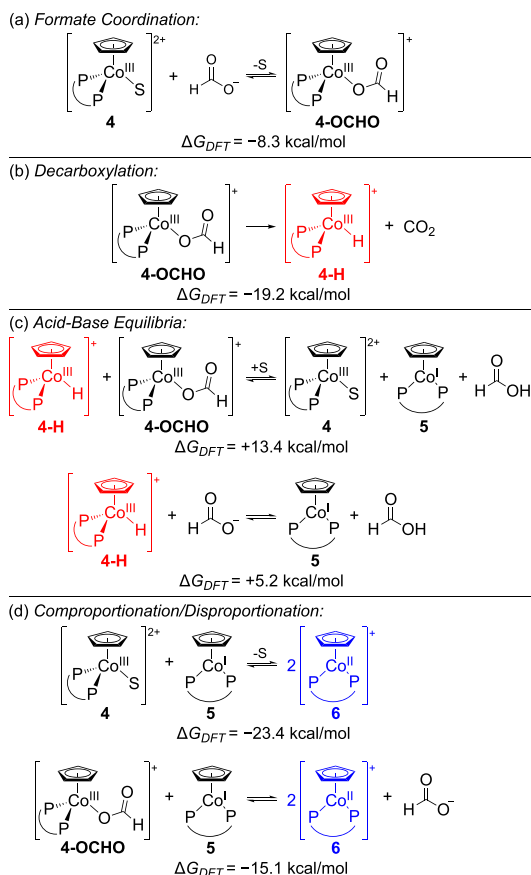
Figure 4. (a) Reactivity of **1–4** with formate. (b) ^1H NMR of the reaction of **4** with formate: **4** (black), and formation of **4-OCHO** (blue; after formate addition at 25 °C), **6** (green; after 1 h at 65 °C), and **4-H** (red; after 13.5 h at 65 °C). Formate added as $[\text{NBu}_4][\text{HCO}_2]\cdot\text{HCO}_2\text{H}$.

Experimental Details). Specifically, we observe a slight upfield shift of the Cp and methyl resonances, as well as a new triplet signal ($^4J_{\text{PH}} = 5$ Hz) at 7.67 ppm that is assigned to the proton on a coordinated formate ligand. This proposed formate adduct, **4-OCHO**, is surprisingly stable at 25 °C, showing almost no change over 24 h by ^1H NMR spectroscopy. However, heating a solution of **4-OCHO** at 65 °C results in the disappearance of this species over 90 min and the appearance of broad paramagnetic resonances. Diamagnetic signals from **4-H** gradually grow in over the course of 13.5 h with the simultaneous decay of the paramagnetic product. The final conversion to **4-H** was determined to be $72 \pm 5\%$ by integration of the Cp, methyl, and hydride signals versus an internal standard (hexamethyldisiloxane). In a larger scale experiment, a solution of **4** and $[\text{NBu}_4][\text{HCO}_2]\cdot\text{HCO}_2\text{H}$ (1 equiv) in MeCN was heated to 60 °C in a sealed flask. Analysis of the flask headspace by gas chromatography after 5 h showed CO_2 production with $74 \pm 10\%$ conversion, confirming that the formation of **4-H** proceeds with formate decarboxylation (see Supporting Information for Experimental Details). Notably, negligible CO_2 production is observed in the absence of **4** under otherwise identical conditions. These data show that **4** is capable of facilitating formate oxidation via hydride

transfer and that decomposition of the metal complex is minimal under these conditions. However, the rate of the stoichiometric reaction of **4** with formate is slow, even at elevated temperatures. Given these shortcomings, **4** was not explored further as a catalyst for formate oxidation.

Mechanistic Considerations. A proposed mechanism for the formation of a paramagnetic species and delayed onset of 4-H production is shown in Scheme 6. Initial coordination of

Scheme 6. Proposed Reaction Steps and Calculated Free Energies for the Conversion of **4 to **6** and 4-H (S = acetonitrile)**

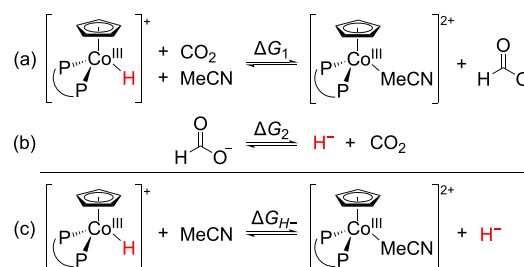


formate is rapid (Scheme 6a), and decarboxylation of 4-OCHO would release CO₂ and generate 4-H (Scheme 6b); however, this step is slow, allowing for excess formate or 4-OCHO to quickly deprotonate 4-H as soon as it is generated (Scheme 6c). While the estimated pK_a of formic acid in acetonitrile (20.9)⁶⁶ is lower than that of 4-H, we note that this value is not accurately established, and the deprotonation equilibrium will be initially driven forward by the relatively high concentration of base compared to the small amount of 4-H. This deprotonation yields formic acid and the neutral Co^I complex **5**, which is not observed during the reaction likely due to its limited solubility in acetonitrile. The presence of both Co^{III} (as **4** and/or 4-OCHO) and Co^I species will result in rapid comproportionation to yield the paramagnetic Co^{II} complex, [(Medcpa)CpCo][PF₆], **6** (Scheme 6d). This process should be favorable based on the difference in the Co^{III/II} and Co^{II/I} reduction potentials ($K_{\text{eq}} \sim 5 \times 10^{11}$). Complex **6** was independently synthesized via one electron reduction of **4** with KC₈ (1 equiv, see Supporting

Information), and its ¹H NMR spectrum in MeCN-*d*₃ matches the paramagnetic species observed during formate oxidation (Figures 4b and S24). After consumption of 4-OCHO, comproportionation is no longer accessible, and instead the equilibrium will favor disproportionation of **6** followed by protonation of **5** with formic acid. These reversible equilibria account for the decrease in the concentration of **6** and the accumulation of 4-H at later times.

Density functional theory (DFT) was employed to further validate our measurements of the thermodynamic hydride accepting ability of 1–4 as well as the mechanism of formate oxidation. The bond lengths and angles of the calculated structures of 1–4 were found to be in good agreement with the single crystal X-ray structures (Table S7). To mitigate the difficulties of accurately calculating the absolute free energy of the hydride anion, we used the isodesmic reactions shown in Scheme 7 to obtain computed hydricity values for 1-H–4-H.

Scheme 7. Isodesmic Reaction for Determining Hydricity of 1-H–4-H



These results are summarized in Table 3: for all complexes, there is good agreement between the computed hydricities and our experimentally determined values.

Table 3. Measured and Calculated Hydricities of 1-H–4-H at 25°C

complex	hydricity (kcal/mol)	
	measured	calculated ^c
1-H	71.0 ^a	72.9
2-H	73.8 ^a	72.6
3-H	71.7 ^a	73.3
4-H	71.0 ^b	71.7

^aHydricity derived from the *in situ* deprotonation of the Co–hydride complex. ^bHydricity derived spectrometrically from the titration of 4-H with DBU. ^cHydricity calculated from the isodesmic reaction shown in Scheme 7. Level of theory: M06-L/def2-TZVPP (Co)/def2-TZVP (C, H, N, P)/def2-TZVPD (C, H, O of formate).^{67–70}

Our calculations predict that the decarboxylation of formate by **4** to yield CO₂ and 4-H is overall exergonic by 27.5 kcal/mol (Scheme 6). In good agreement with our proposed reaction sequence and experimental results, initial formation of 4-OCHO is thermodynamically favorable by 8.3 kcal/mol, and subsequent hydride transfer generation of 4-H and CO₂ is downhill by 19.2 kcal/mol. Once 4-H is generated, it can be deprotonated by either 4-OCHO or free formate (Scheme 6c). While both of these reactions are predicted to be slightly endergonic at room temperature, we expect both deprotonation equilibria to be readily accessible at the elevated reaction temperature used experimentally, and the low initial concentrations of 4-H will shift these equilibria toward product

formation. The subsequent comproportionation of the Co^{III} and Co^{I} complexes is calculated to be favorable (Scheme 6d) and is consistent with the initial accumulation of paramagnetic **6** observed during the reaction (Figures 4b and S34).

Despite the large predicted thermodynamic driving force for formate oxidation, elevated temperatures are required to induce the hydride transfer step with **4**, suggesting that a large kinetic barrier hinders this reaction. It is also clear from our studies that the instability of **1–3** and their associated hydride complexes in the presence of formate precludes their use as formate oxidation catalysts. However, with complex **4**, we have demonstrated all key steps to establish an electrocatalytic cycle for formate oxidation (Scheme 1): formate decarboxylation via hydride transfer to the metal, rapid deprotonation of the resulting Co^{III} –hydride by an excess of formate, and facile electrochemical oxidation of Co^{I} to regenerate **4** at the electrode. The improved stability of **4** under these reaction conditions may be due to greater steric protection from the bulky cyclohexyl groups, as well as the lower acidity of **4-H** that may disfavor proton transfer to the Cp ligand and subsequent decomposition to release cyclopentadiene.⁷¹ Future investigations will further probe the detailed mechanism of formate decarboxylation at **4** using computational studies and will explore alternative ligand designs at cobalt that maintain similar thermodynamic properties as these bis(phosphino)amine systems but provide greater stability of the metal complex under electrocatalytic conditions and mediate faster reactivity for hydride transfer.

CONCLUSION

In summary, we have synthesized and structurally characterized a series of Co^{III} half-sandwich complexes supported by bis(phosphino)amine ligands. The thermodynamic hydride accepting ability of these compounds was determined through spectroscopic and DFT computational methods. On the basis of these values, all complexes in this series were predicted to favor hydride transfer from formate and the oxidative release of CO_2 with high exergonicity. Indeed, with heating, stoichiometric hydride transfer from formate to **4** was observed, concomitant with the extrusion of CO_2 . It was hypothesized that the pendent amine group in the bis(phosphino)amine ligands would facilitate facile formate oxidation akin to other amine-functionalized phosphine ligands. However, the kinetic barrier for this step remains prohibitively high, indicating the poor capacity of the bis(phosphino)amine ligand system to assist in achieving rapid reactivity. We are further exploring the role that pendent amine groups may play for facilitating facile and rapid hydride transfer with other ligand architectures as we continue to investigate formate electro-oxidation with first-row transition metal compounds.

ASSOCIATED CONTENT

Supporting Information

The Supporting Information is available free of charge at <https://pubs.acs.org/doi/10.1021/acs.inorgchem.1c00563>.

Experimental procedures, crystallographic details, additional data, computational methods, and Cartesian coordinates for DFT calculated structures (PDF)

Accession Codes

CDCC 2064461–2064466 contains the supplemental crystallographic data for this paper. These data can be obtained free of charge via www.ccdc.cam.ac.uk/data_request/cif, or by

emailing data_request@ccdc.cam.ac.uk, or by contacting The Cambridge Crystallographic Data Centre, 12 Union Road, Cambridge CB2 1EZ, UK; fax: + 44 1223 336033.

AUTHOR INFORMATION

Corresponding Author

Kate M. Waldie – Department of Chemistry and Chemical Biology, Rutgers, The State University of New Jersey, New Brunswick, New Jersey 08903, United States; orcid.org/0000-0001-6444-6122; Email: kate.waldie@rutgers.edu

Authors

Andrew W. Cook – Department of Chemistry and Chemical Biology, Rutgers, The State University of New Jersey, New Brunswick, New Jersey 08903, United States; orcid.org/0000-0002-8850-8946

Thomas J. Emge – Department of Chemistry and Chemical Biology, Rutgers, The State University of New Jersey, New Brunswick, New Jersey 08903, United States

Complete contact information is available at:

<https://pubs.acs.org/doi/10.1021/acs.inorgchem.1c00563>

Author Contributions

The manuscript was written through contributions of all authors. All authors have given approval to the final version of the manuscript.

Notes

The authors declare no competing financial interest.

ACKNOWLEDGMENTS

The authors thank Rutgers, The State University of New Jersey, for generous funding support. The authors acknowledge the Office of Advanced Research Computing (OARC) at Rutgers, The State University of New Jersey, for providing access to the Amarel cluster and associated research computing resources that have contributed to the results reported here.

REFERENCES

- (1) Eberle, U.; Felderhoff, M.; Schüth, F. Chemical and Physical Solutions for Hydrogen Storage. *Angew. Chem., Int. Ed.* **2009**, *48*, 6608–6630.
- (2) Andrews, J.; Shabani, B. Where does Hydrogen Fit in a Sustainable Energy Economy? *Procedia Eng.* **2012**, *49*, 15–25.
- (3) Taheri Najafabadi, A. CO_2 chemical conversion to useful products: An engineering insight to the latest advances toward sustainability. *Int. J. Energy Res.* **2013**, *37*, 485–499.
- (4) Cook, A. W.; Waldie, K. M. Molecular Electrocatalysts for Alcohol Oxidation: Insights and Challenges for Catalyst Design. *ACS Appl. Energy Mater.* **2020**, *3*, 38–46.
- (5) Grasemann, M.; Laurenczy, G. Formic acid as a hydrogen source – recent developments and future trends. *Energy Environ. Sci.* **2012**, *5*, 8171–8181.
- (6) An, L.; Chen, R. Direct formate fuel cells: A review. *J. Power Sources* **2016**, *320*, 127–139.
- (7) Singh, A. K.; Singh, S.; Kumar, A. Hydrogen energy future with formic acid: a renewable chemical hydrogen storage system. *Catal. Sci. Technol.* **2016**, *6*, 12–40.
- (8) Alig, L.; Fritz, M.; Schneider, S. First-Row Transition Metal (De)Hydrogenation Catalysis Based On Functional Pincer Ligands. *Chem. Rev.* **2019**, *119*, 2681–2751.
- (9) Boddien, A.; Mellmann, D.; Gärtner, F.; Jackstell, R.; Junge, H.; Dyson, P. J.; Laurenczy, G.; Ludwig, R.; Beller, M. Efficient Dehydrogenation of Formic Acid Using an Iron Catalyst. *Science* **2011**, *333*, 1733–1736.

- (10) Zell, T.; Butschke, B.; Ben-David, Y.; Milstein, D. Efficient Hydrogen Liberation from Formic Acid Catalyzed by a Well-Defined Iron Pincer Complex Under Mild Conditions. *Chem. - Eur. J.* **2013**, *19*, 8068–8072.
- (11) Bielinski, E. A.; Lagaditis, P. O.; Zhang, Y.; Mercado, B. Q.; Würtele, C.; Bernskoetter, W. H.; Hazari, N.; Schneider, S. Lewis Acid-Assisted Formic Acid Dehydrogenation Using a Pincer-Supported Iron Catalyst. *J. Am. Chem. Soc.* **2014**, *136*, 10234–10237.
- (12) Tondreau, A. M.; Boncella, J. M. 1,2-Addition of Formic or Oxalic Acid to $-N\{CH_2CH_2(PiPr_2)\}_2$ -Supported Mn(I) Dicarbonyl Complexes and the Manganese-Mediated Decomposition of Formic Acid. *Organometallics* **2016**, *35*, 2049–2052.
- (13) Mellone, I.; Gorgas, N.; Bertini, F.; Peruzzini, M.; Kirchner, K.; Gonsalvi, L. Selective Formic Acid Dehydrogenation Catalyzed by Fe-PNP Pincer Complexes Based on the 2,6-Diaminopyridine Scaffold. *Organometallics* **2016**, *35*, 3344–3349.
- (14) Galan, B. R.; Schoffel, J.; Linehan, J. C.; Seu, C.; Appel, A. M.; Roberts, J. A.; Helm, M. L.; Kilgore, U. J.; Yang, J. Y.; DuBois, D. L.; Kubiak, C. P. Electrocatalytic Oxidation of Formate by $[Ni(P^R_2N^R_2)_2(CH_3CN)]^{2+}$ Complexes. *J. Am. Chem. Soc.* **2011**, *133*, 12767–12779.
- (15) Sordakis, K.; Tang, C.; Vogt, L. K.; Junge, H.; Dyson, P. J.; Beller, M.; Laurenczy, G. Homogeneous Catalysis for Sustainable Hydrogen Storage in Formic Acid and Alcohols. *Chem. Rev.* **2018**, *118*, 372–433.
- (16) Guan, C.; Zhang, D. D.; Pan, Y.; Iguchi, M.; Ajitha, M. J.; Hu, J.; Li, H.; Yao, C.; Huang, M. H.; Min, S.; Zheng, J.; Himeda, Y.; Kawanami, H.; Huang, K. W. Dehydrogenation of Formic Acid Catalyzed by a Ruthenium Complex with an N,N' -Diimine Ligand. *Inorg. Chem.* **2017**, *56*, 438–445.
- (17) Fidalgo, J.; Ruiz-Castaneda, M.; Garcia-Herbosa, G.; Carbayo, A.; Jalon, F. A.; Rodriguez, A. M.; Manzano, B. R.; Espino, G. Versatile Rh- and Ir-Based Catalysts for CO_2 Hydrogenation, Formic Acid Dehydrogenation, and Transfer Hydrogenation of Quinolines. *Inorg. Chem.* **2018**, *57*, 14186–14198.
- (18) Nakajima, T.; Kamiyoy, Y.; Kishimoto, M.; Imai, K.; Nakamae, K.; Ura, Y.; Tanase, T. Synergistic Cu_2 Catalysts for Formic Acid Dehydrogenation. *J. Am. Chem. Soc.* **2019**, *141*, 8732–8736.
- (19) Hong, D.; Shimoyama, Y.; Ohgomi, Y.; Kanega, R.; Kotani, H.; Ishizuka, T.; Kon, Y.; Himeda, Y.; Kojima, T. Cooperative Effects of Heterodinuclear $Ir^{III}-M^{II}$ Complexes on Catalytic H_2 Evolution from Formic Acid Dehydrogenation in Water. *Inorg. Chem.* **2020**, *59*, 11976–11985.
- (20) Shin, H.; Liu, X.; Lacelle, T.; MacDonell, R. J.; Schuurman, M. S.; Malenfant, P. R. L.; Paquet, C. Mechanistic Insight into Bis(amino) Copper Formate Thermochemistry for Conductive Molecular Ink Design. *ACS Appl. Mater. Interfaces* **2020**, *12*, 33039–33049.
- (21) Kanega, R.; Ertem, M. Z.; Onishi, N.; Szalda, D. J.; Fujita, E.; Himeda, Y. CO_2 Hydrogenation and Formic Acid Dehydrogenation Using Ir Catalysts with Amide-Based Ligands. *Organometallics* **2020**, *39*, 1519–1531.
- (22) Kawanami, H.; Iguchi, M.; Himeda, Y. Ligand Design for Catalytic Dehydrogenation of Formic Acid to Produce High-pressure Hydrogen Gas under Base-free Conditions. *Inorg. Chem.* **2020**, *59*, 4191–4199.
- (23) Lentz, N.; Aloisi, A.; Thuéry, P.; Nicolas, E.; Cantat, T. Additive-Free Formic Acid Dehydrogenation Catalyzed by a Cobalt Complex. *Organometallics* **2021**, *40*, 565–569.
- (24) Liu, H.; Wang, W. H.; Xiong, H.; Nijamudheen, A.; Ertem, M. Z.; Wang, M.; Duan, L. Efficient Iridium Catalysts for Formic Acid Dehydrogenation: Investigating the Electronic Effect on the Elementary β -Hydride Elimination and Hydrogen Formation Steps. *Inorg. Chem.* **2021**, *60*, 3410–3417.
- (25) Rakowski DuBois, M.; DuBois, D. L. The roles of the first and second coordination spheres in the design of molecular catalysts for H_2 production and oxidation. *Chem. Soc. Rev.* **2009**, *38*, 62–72.
- (26) Chabolla, S. A.; Yang, J. Y. For CO_2 Reduction, Hydrogen-Bond Donors Do the Trick. *ACS Cent. Sci.* **2018**, *4*, 315–317.
- (27) Gimbert, Y.; Robert, F.; Durif, A.; Averbuch, M. T.; Kann, N.; Greene, A. E. Synthesis and Characterization of New Binuclear $Co(0)$ Complexes with Diphosphinoamine Ligands. A Potential Approach for Asymmetric Pauson-Khand Reactions. *J. Org. Chem.* **1999**, *64*, 3492–3497.
- (28) Daly, S.; Haddow, M. F.; Orpen, A. G.; Rolls, G. T. A.; Wass, D. F.; Wingad, R. L. Copper(I) Diphosphine Catalysts for C–N Bond Formation: Synthesis, Structure, and Ligand Effects. *Organometallics* **2008**, *27*, 3196–3202.
- (29) Aydemir, M.; Durap, F.; Baysal, A.; Akba, O.; Gümgüm, B.; Özkar, S.; Yıldırım, L. T. Synthesis and characterization of new bis(diphenylphosphino)aniline ligands and their complexes: X-ray crystal structure of palladium(II) and platinum(II) complexes, and application of palladium(II) complexes as pre-catalysts in Heck and Suzuki cross-coupling reactions. *Polyhedron* **2009**, *28*, 2313–2320.
- (30) Ghosh, S.; Hogarth, G.; Hollingsworth, N.; Holt, K. B.; Richards, I.; Richmond, M. G.; Sanchez, B. E.; Unwin, D. Models of the iron-only hydrogenase: a comparison of chelate and bridge isomers of $Fe_2(CO)_4\{Ph_2PN(R)PPh_2\}(\mu\text{-pdt})$ as proton-reduction catalysts. *Dalton Trans.* **2013**, *42*, 6775–6792.
- (31) Song, L. C.; Li, J. P.; Xie, Z. J.; Song, H. B. Synthesis, Structural Characterization, and Electrochemical Properties of Dinuclear Ni/Mn Model Complexes for the Active Site of [NiFe]-Hydrogenases. *Inorg. Chem.* **2013**, *52*, 11618–11626.
- (32) Zhao, P.-H.; Ma, Z.-Y.; Hu, M.-Y.; He, J.; Wang, Y.-Z.; Jing, X.-B.; Chen, H.-Y.; Wang, Z.; Li, Y.-L. PNP-Chelated and -Bridged Diiron Dithiolate Complexes $Fe_2(\mu\text{-pdt})(CO)_4\{(Ph_2P)_2NR\}$ Together with Related Monophosphine Complexes for the $[2Fe]_H$ Subsite of [FeFe]-Hydrogenases: Preparation, Structure, and Electrocatalysis. *Organometallics* **2018**, *37*, 1280–1290.
- (33) Cooley, N. A.; Green, S. M.; Wass, D. F.; Heslop, K.; Orpen, A. G.; Pringle, P. G. Nickel Ethylene Polymerization Catalysts Based on Phosphorus Ligands. *Organometallics* **2001**, *20*, 4769–4771.
- (34) Agapie, T.; Schofer, S. J.; Labinger, J. A.; Bercaw, J. E. Mechanistic Studies of the Ethylene Trimerization Reaction with Chromium-Diphosphine Catalysts: Experimental Evidence for a Mechanism Involving Metallacyclic Intermediates. *J. Am. Chem. Soc.* **2004**, *126*, 1304–1305.
- (35) Bollmann, A.; Blann, K.; Dixon, J. T.; Hess, F. M.; Killian, E.; Maumela, H.; McGuinness, D. S.; Morgan, D. H.; Neveling, A.; Otto, S.; Overett, M.; Slawin, A. M. Z.; Wasserscheid, P.; Kuhlmann, S. Ethylene Tetramerization: A New Route to Produce 1-Octene in Exceptionally High Selectivities. *J. Am. Chem. Soc.* **2004**, *126*, 14712–14713.
- (36) Blann, K.; Bollmann, A.; Debod, H.; Dixon, J.; Killian, E.; Nongodlwana, P.; Maumela, M.; Maumela, H.; McConnell, A.; Morgan, D. Ethylene tetramerization: Subtle effects exhibited by N-substituted diphosphinoamine ligands. *J. Catal.* **2007**, *249*, 244–249.
- (37) DuBois, D. L.; Berning, D. E. Hydricity of transition-metal hydrides and its role in CO_2 reduction. *Appl. Organomet. Chem.* **2000**, *14*, 860–862.
- (38) Curtis, C. J.; Miedaner, A.; Ciancanelli, R.; Ellis, W. W.; Noll, B. C.; Rakowski DuBois, M.; DuBois, D. L. $[Ni(Et_2PCH_2NMeCH_2PEt_2)_2]^{2+}$ as a Functional Model for Hydrogenases. *Inorg. Chem.* **2003**, *42*, 216–227.
- (39) Waldie, K. M.; Ostericher, A. L.; Reineke, M. H.; Sasayama, A. F.; Kubiak, C. P. Hydricity of Transition-Metal Hydrides: Thermodynamic Considerations for CO_2 Reduction. *ACS Catal.* **2018**, *8*, 1313–1324.
- (40) Dempsey, J. L.; Brunschwig, B. S.; Winkler, J. R.; Gray, H. B. Hydrogen Evolution Catalyzed by Cobaloximes. *Acc. Chem. Res.* **2009**, *42*, 1995–2004.
- (41) Marinescu, S. C.; Winkler, J. R.; Gray, H. B. Molecular mechanisms of cobalt-catalyzed hydrogen evolution. *Proc. Natl. Acad. Sci. U. S. A.* **2012**, *109*, 15127–15131.
- (42) McKone, J. R.; Marinescu, S. C.; Brunschwig, B. S.; Winkler, J. R.; Gray, H. B. Earth-abundant hydrogen evolution electrocatalysts. *Chem. Sci.* **2014**, *5*, 865–878.

- (43) Kaeffer, N.; Chavarot-Kerlidou, M.; Artero, V. Hydrogen Evolution Catalyzed by Cobalt Diimine-Dioxime Complexes. *Acc. Chem. Res.* **2015**, *48*, 1286–1295.
- (44) Elgrishi, N.; Kurtz, D. A.; Dempsey, J. L. Reaction Parameters Influencing Cobalt Hydride Formation Kinetics: Implications for Benchmarking H₂-Evolution Catalysts. *J. Am. Chem. Soc.* **2017**, *139*, 239–244.
- (45) Roy, S.; Sharma, B.; Pecaut, J.; Simon, P.; Fontecave, M.; Tran, P. D.; Derat, E.; Artero, V. Molecular Cobalt Complexes with Pendant Amines for Selective Electrocatalytic Reduction of Carbon Dioxide to Formic Acid. *J. Am. Chem. Soc.* **2017**, *139*, 3685–3696.
- (46) Queyriaux, N.; Sun, D.; Fize, J.; Pecaut, J.; Field, M. J.; Chavarot-Kerlidou, M.; Artero, V. Electrocatalytic Hydrogen Evolution with a Cobalt Complex Bearing Pendant Proton Relays: Acid Strength and Applied Potential Govern Mechanism and Stability. *J. Am. Chem. Soc.* **2020**, *142*, 274–282.
- (47) Balakrishna, M. S.; Reddy, V. S.; Krishnamurthy, S. S.; Nixon, J. F.; Burckett St. Laurent, J. C. T. R. Coordination chemistry of diphosphinoamine and cyclodiphosphazane ligands. *Coord. Chem. Rev.* **1994**, *129*, 1–90.
- (48) Pernik, I.; Hooper, J. F.; Chaplin, A. B.; Weller, A. S.; Willis, M. C. Exploring Small Bite-Angle Ligands for the Rhodium-Catalyzed Intermolecular Hydroacylation of β -S-Substituted Aldehydes with 1-Octene and 1-Octyne. *ACS Catal.* **2012**, *2*, 2779–2786.
- (49) Koelle, U. Darstellung und redox-eigenschaften dikationischer kobalthalbsandwichkomplexe. *J. Organomet. Chem.* **1980**, *184*, 379–383.
- (50) Landon, S. J.; Brill, T. B. Steric and Electronic Control of the Arbusov Reaction in Transition-Metal Halides: ¹H and ³¹P NMR Study of the Reaction of [CpCo(LL)X]⁺ complexes (LL = N, P, As chelate ligands; X⁻ = Cl⁻, Br⁻, I⁻, CN⁻) with P(OMe)₃. *Inorg. Chem.* **1984**, *23*, 1266–1271.
- (51) Bao, Q. B.; Landon, S. J.; Rheingold, A. L.; Haller, T. M.; Brill, T. B. Comparison of the Self-Reactivity of [CpCo(PP)I]⁺ Complexes, PP = Ph₂P(CH₂)_nPPh₂ (n = 1–4), Leading to Bridged and Oxidized Dangling PP. Reactions, Spectral Studies, and Structures of [CpCo(dppm)I]I₂, CpCo[dppm(O)]I₂, and Cp₂Co₂I₄(μ -dppm). *Inorg. Chem.* **1985**, *24*, 900–908.
- (52) Kuhn, N.; Brüggemann, H.; Winter, M.; De Bellis, V. M. Synthese und reaktivität von dienylnmetall-verbindingen: XXVII. Ein einfacher weg zur synthese von cyclopentadienylcobalt(III)-dikationen. *J. Organomet. Chem.* **1987**, *320*, 391–400.
- (53) Garcia, M. H.; Mendes, P. J.; Dias, A. R. Synthesis and electrochemical studies of organometallic cobalt(III) complexes with substituted benzonitrile chromophores: NMR spectroscopic data as a probe on the second-order non-linear optical properties. *J. Organomet. Chem.* **2005**, *690*, 4063–4071.
- (54) Nagasawa, T.; Nagata, T. Synthesis and electrochemistry of Co(III) and Co(I) complexes having C₅Me₅ auxiliary. *Biochim. Biophys. Acta, Bioenerg.* **2007**, *1767*, 666–670.
- (55) Waldie, K. M.; Ramakrishnan, S.; Kim, S. K.; Maclaren, J. K.; Chidsey, C. E.; Waymouth, R. M. Multielectron Transfer at Cobalt: Influence of the Phenylazopyridine Ligand. *J. Am. Chem. Soc.* **2017**, *139*, 4540–4550.
- (56) Waldie, K. M.; Kim, S.-K.; Ingram, A. J.; Waymouth, R. M. Cyclopentadienyl Cobalt Complexes as Precatalysts for Electrocatalytic Hydrogen Evolution. *Eur. J. Inorg. Chem.* **2017**, *2017*, 2755–2761.
- (57) Koelle, U.; Paul, S. Electrochemical Reduction of Protonated Cyclopentadienylcobalt Phosphine Complexes. *Inorg. Chem.* **1986**, *25*, 2689–2694.
- (58) Werner, H.; Lippert, F.; Peters, K.; Schnering, H. G. V. Synthese und Reaktionen der Metall-Base [(C₅Me₄H)Co(PMe₃)₂]. *Chem. Ber.* **1992**, *125*, 347–352.
- (59) Hapke, M.; Kral, K.; Fischer, C.; Spannenberg, A.; Gutnov, A.; Redkin, D.; Heller, B. Asymmetric Synthesis of Axially Chiral 1-aryl-5,6,7,8-tetrahydroquinolines by Cobalt-Catalyzed [2 + 2 + 2] Cycloaddition Reaction of 1-aryl-1,7-octadiynes and Nitriles. *J. Org. Chem.* **2010**, *75*, 3993–4003.
- (60) Cotton, F. A.; Kühn, F. E.; Yokochi, A. Synthesis and structure of trans-[di(μ -acetato)dichlorodi-(μ -bis(diphenylphosphino)methylamine)dimolybdenum(II)] and the structure of bis-(diphenylphosphino)methylamine. *Inorg. Chim. Acta* **1996**, *252*, 251–256.
- (61) Fei, Z.; Scopelliti, R.; Dyson, P. J. Influence of the functional group on the synthesis of aminophosphines, diphosphinoamines and iminobiphosphines. *Dalton Trans.* **2003**, 2772.
- (62) Liu, X. F.; Xu, W. H.; Li, H. N,N-Bis(diphenyl-Phosphanyl)benzyl-amine. *Acta Crystallogr., Sect. E: Struct. Rep. Online* **2011**, *67*, o370.
- (63) Dudeney, N.; Green, J. C.; Grebenik, P.; Kirchner, O. N. Synthesis and structural characterization of the electron rich complexes Co(η -C₅Me₅)(R₂PCH₂CH₂PR₂) (R = Me, Ph); photoelectron spectroscopic studies of some pentamethylcyclopentadienylphosphinecobalt complexes. *J. Organomet. Chem.* **1983**, *252*, 221–229.
- (64) Wiedner, E. S.; Chambers, M. B.; Pitman, C. L.; Bullock, R. M.; Miller, A. J.; Appel, A. M. Thermodynamic Hydricity of Transition Metal Hydrides. *Chem. Rev.* **2016**, *116*, 8655–8692.
- (65) Kaljurand, I.; Kütt, A.; Sooväli, L.; Rodima, T.; Mäemets, V.; Leito, I.; Koppel, I. A. Extension of the Self-Consistent Spectrophotometric Basicity Scale in Acetonitrile to a Full Span of 28 pKa Units: Unification of Different Basicity Scales. *J. Org. Chem.* **2005**, *70*, 1019–1028.
- (66) Stirling, M. J.; Sweeney, G.; MacRory, K.; Blacker, A. J.; Page, M. I. The kinetics and mechanism of the organo-iridium-catalysed enantioselective reduction of imines. *Org. Biomol. Chem.* **2016**, *14*, 3614–3622.
- (67) Frisch, M. J.; Trucks, G. W.; Schlegel, H. B.; Scuseria, G. E.; Robb, M. A.; Cheeseman, J. R.; Scalmani, G.; Barone, V.; Petersson, G. A.; Nakatsuji, H.; Li, X.; Caricato, M.; Marenich, A. V.; Bloino, J.; Janesko, B. G.; Gomperts, R.; Mennucci, B.; Hratchian, H. P.; Ortiz, J. V.; Izmaylov, A. F.; Sonnenberg, J. L.; Williams-Young, D.; Ding, F.; Lipparini, F.; Egidi, F.; Goings, J.; Peng, B.; Petrone, A.; Henderson, T.; Ranasinghe, D.; Zakrzewski, V. G.; Gao, J.; Rega, N.; Zheng, G.; Liang, W.; Hada, M.; Ehara, M.; Toyota, K.; Fukuda, R.; Hasegawa, J.; Ishida, M.; Nakajima, T.; Honda, Y.; Kitao, O.; Nakai, H.; Vreven, T.; Throssell, K.; Montgomery, J. A., Jr.; Peralta, J. E.; Ogliaro, F.; Bearpark, M. J.; Heyd, J. J.; Brothers, E. N.; Kudin, K. N.; Staroverov, V. N.; Keith, T. A.; Kobayashi, R.; Normand, J.; Raghavachari, K.; Rendell, A. P.; Burant, J. C.; Iyengar, S. S.; Tomasi, J.; Cossi, M.; Millam, J. M.; Klene, M.; Adamo, C.; Cammi, R.; Ochterski, J. W.; Martin, R. L.; Morokuma, K.; Farkas, O.; Foresman, J. B.; Fox, D. J. *Gaussian 16*, revision A.03; Gaussian, Inc.: Wallingford, CT, 2016.
- (68) Weigend, F.; Ahlrichs, R. Balanced basis sets of split valence, triple zeta valence and quadruple zeta valence quality for H to Rn: Design and assessment of accuracy. *Phys. Chem. Chem. Phys.* **2005**, *7*, 3297–3305.
- (69) Rappoport, D.; Furche, F. Property-optimized gaussian basis sets for molecular response calculations. *J. Chem. Phys.* **2010**, *133*, 134105.
- (70) Pritchard, B. P.; Altarawy, D.; Didier, B.; Gibson, T. D.; Windus, T. L. A New Basis Set Exchange: An Open, Up-to-Date Resource for the Molecular Sciences Community. *J. Chem. Inf. Model.* **2019**, *59*, 4814–4820.
- (71) Kurtz, D. A.; Dhar, D.; Elgrishi, N.; Kandemir, B.; McWilliams, S. F.; Howland, W. C.; Chen, C. H.; Dempsey, J. L. Redox-Induced Structural Reorganization Dictates Kinetics of Cobalt(III) Hydride Formation via Proton-Coupled Electron Transfer. *J. Am. Chem. Soc.* **2021**, *143*, 3393–3406.

NOTE ADDED AFTER ASAP PUBLICATION

This article was published ASAP on April 27, 2021. Schemes 1, 4, 6, and 7 have been updated and the corrected version was reposted on April 28, 2021.